Optics and Lasers in Engineering 119 (2019) 56–64

Contents lists available at ScienceDirect

Optics and Lasers in Engineering

journal homepage: www.elsevier.com/locate/optlaseng

Statistical evaluation method to determine the laser welding depth by optical coherence tomography

Meiko Boley*, Florian Fetzer, Rudolf Weber, Thomas Graf

Institut für Strahlwerkzeuge, Universität Stuttgart, Stuttgart 70569, Germany

ARTICLE INFO

Keywords:
Laser welding
depth measurement
Optical coherence tomography (OCT)
Inline coherent imaging (ICI)
Welding depth
Online penetration depth measurement

ABSTRACT

A statistical filtering method to determine the depth of laser-welded seams from signals recorded by means of optical coherence tomography (OCT) is proposed and discussed. The measured data points are initially classified into noise and significant data by means of a noise probability, which was defined based on the normalized Poisson distribution. A percentile filter is then applied to the significant data to obtain the depth of the weld seam. It is shown that the depth determined by this approach corresponds to the real seam depth, as obtained from longitudinal sections, to within an average error of less than 5%. The method can be applied to different laser welding situations without having to adjust the filter parameters.

1. Introduction

A precise online measurement of the welding depth during laser beam welding is of major importance especially for quality assurance. Depending on the geometries of the welded parts and the requirements for the documentation of the quality control this can become an increasingly challenging task.

Information on the penetration depth which is reached during laser welding can be gained by measuring the length of the vapor capillary. However, reliable measurements of the depths of the vapor capillary are challenging due to the rough environment, which is influenced by dust, spatters, thermal radiation and a rapidly changing geometry of the capillary itself. Reliable measurements should therefore be unaffected by this environment and feature acquisition rates in the kHz range.

Many different approaches have been proposed and investigated to determine the depth of the weld seam by means of photodiodes, spectrometers and camera systems. It has been shown that there exists a correlation between the back reflection measured by photodiodes and the weld seam depth [1–3]. An approach that measures the infrared radiation emitted from the capillary with a photodiode and allows to control the depth of the weld seam by adapting the laser power is presented in [4]. When welding dissimilar materials in an overlap configuration, the spectrum of the thermal emission changes when the capillary extends from the first to the second sheet which can be used the asses and control the depth of the weld seam [5]. A camera-based approach, where the lower opening of the keyhole was monitored during full-penetration welding to control the laser power, is presented in [6,7]. The same was found to also be applicable to control the partial penetration into the lower sheet in overlap configuration. Although these methods have been used successfully in some cases, they do not provide a direct measurement of the varying depth of the vapor capillary. Optical coherence tomography (OCT) [8,9], by contrast, is a well-established method for measuring optical path lengths. Compared to the indirect approaches shown before, the application of OCT to laser beam welding has the main benefits of directly measuring the depth of the capillary, a high tolerance against process emissions and a high measurement rate.

Fig. 1 shows the general setup to integrate OCT into a laser welding facility. In the case of the In-Process Depth Meter (IDM) by Precitec [10] used for the investigations, the coherent light source required for the OCT is a superluminescent laser diode (SLD) with a central wavelength of $1540\,nm \pm 20\,nm$ (40 nm full width at half maximum). The SLD is coupled to a single mode fiber. To use the same fiber as a connection from the SLD to the beam splitter and from there back to the spectrometer, the two beam passes are separated by an optical circulator [11]. The beam splitter is used to direct a small fraction of the light towards a reference path, where the light is reflected back to the spectrometer by a mirror. The major fraction of the probe beam from the SLD is directed towards the process head where it is superposed with the processing laser beam and focused onto the workpiece. The probe light that is reflected back from both the reference path and the measurement path is combined and analyzed by a fast spectrometer. The frequency of the interference pattern depends on the length difference between the reference and the measurement path [8,9].

The depth of the weld seam can be measured through the vapor filled capillary, whose depth is only slightly smaller than the seam's depth. According to [12] the melt film below the capillary has a thickness of only

* Corresponding author.
E-mail address: meiko.boley@gmail.com (M. Boley).

https://doi.org/10.1016/j.optlaseng.2019.03.014
Received 19 December 2018; Received in revised form 16 March 2019; Accepted 19 March 2019
Available online 27 March 2019

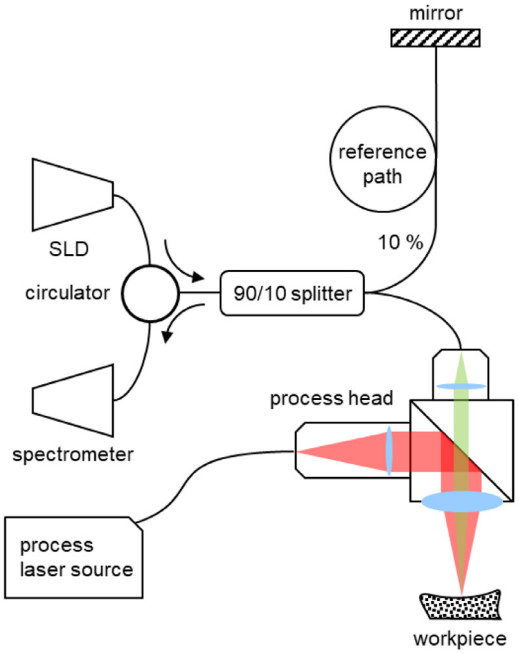

Fig. 1. Optical setup OCT for laser beam welding.

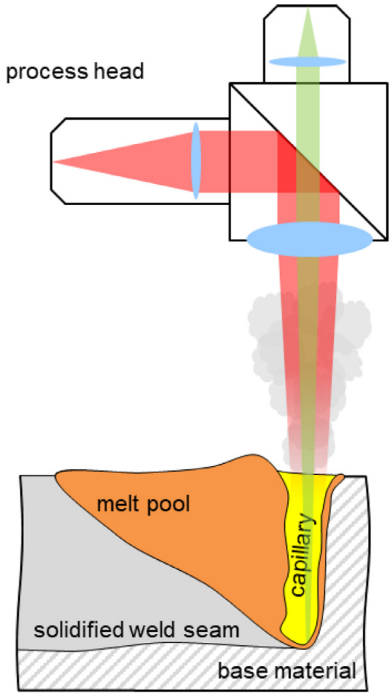

Fig. 2. Process head combining the OCT probe beam (green) with the processing laser beam (red). The OCT probe beam is aligned to hit the deepest point of the capillary.

about 10 µm, which means that for usual welding depths the difference between the seam depth and the length of the capillary is in the order of a few percent.

Fig. 2 shows the processing head with the OCT probe beam (green) that is superimposed with the processing laser beam (red) by means of a dichroic beam splitter. Ideally the OCT beam is aligned in such a way that it hits the capillary's deepest point from where it is reflected back to the sensor.

Since the OCT measures optical path lengths, the influence of the refractive index above and in the capillary has to be taken into account. For the pulsed laser processing of aluminum and copper the refractive index in the volume above the interaction zone was found to range from 0.986 to 1.002 for a beam with a wavelength of 633 nm [13,12]. The temperature of the vapor plume above [14–18] and within [19] the vapor capillary does not exceed 6000 K when welding with lasers with a wavelength of 1 µm, resulting in an only weakly ionized plasma which does not change the refractive index by a significant amount. It can therefore be concluded that the uncertainty of the measurement of the capillary depth using the OCT technique is of the order of only 2%. Indeed it has been shown that the OCT technology has the potential to measure the depth of the vapor-filled capillary which is formed during deep-penetration laser-welding with high accuracy [20–22]. Other applications are the actual control of the capillary depth [10,23–25], autofocus [23], the detection of the breakthrough during laser drilling [23], and 3D laser milling [21,26,27].

In the following it is shown that the optically measured length of the vapor capillary reliably corresponds to the depth of the weld seam, when using a two-step approach to evaluate the OCT signal, which includes a first step to separate the noise and a second step to obtain the weld seam depth.

2. Data acquisition

Two different setups were used for the experimental investigations. A Laserline LDF 4008 laser, whose beam was delivered to the processing head by a fiber with a core diameter of 150 µm, was used an a first setup (setup A). A Precitec YW52 welding head was used with a collimation lens with a focal length of 150 mm and a focusing lens with a focal length of 300 mm. The processing head was inclined by 10° (piercing) to reduce the back-reflection of laser radiation into the beam delivery fiber. The experiments were carried out in ambient air without shielding gas.

The second setup (setup B) consisted of a Trumpf TruDisk 16,002 laser with a wavelength of 1030 nm and a beam delivery fiber with a core diameter of 200 µm. The laser beam was focused by a Precitec YW52 welding head with a collimation lens with a focal length of 200 mm and a focusing lens with a focal length of 200 mm. In this setup the processing head was not inclined as the thin-disk laser is much less sensitive to back-reflections.

Both processing heads where equipped with an In-Process depth meter (IDM). The IDM is an OCT measurement device (as described above), whose probe beam was aligned coaxially to the processing laser beam, so that it measures the depth of the deepest point of the capillary. The measurement rate was 70 kHz and the diameter of the probe beam on the workpiece was 70 µm.

2.1. Raw measurement data

A typical plot of the raw OCT data that was recorded from a welding process in mild steel using setup B with a laser power of $P_L = 2$ kW, a feed rate of $v = 6$ m/min and with the beam focused 3 mm above the surface of the workpiece is shown in Fig. 3. This example will be referred to as example A in the following and is used to explain the data evaluation methods. Other examples will be given later on to illustrate different use-cases. The depth is defined to be negative for points below the surface and positive for points above the surface of the workpiece. Every black dot represents one depth measurement at the given instant in time. The surface, which is measured before and after the welding process, was defined to be zero on the depth scale.

Since the laser was turned on 0.1 s after starting the measurement, the measured depth shown in Fig. 3 is 0 mm during the first 0.1 s. With the capillary opened by the laser at the time $t = 0.1$ s the IDM starts to measure depths mostly ranging below the surface of the workpiece until the laser is turned off after 0.5 s of welding time and the surface is measured again for the remaining measurement time.

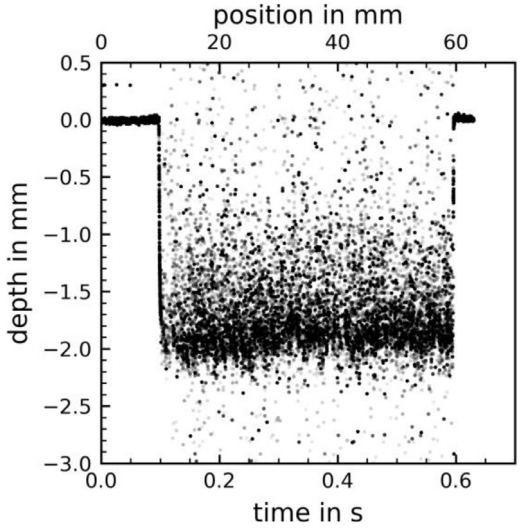

Fig. 3. Raw measurement data acquired during a laser welding process (Example A). Process parameters: Mild steel, v = 6 m/min feed rate, laser power P_L = 2 kW, focal position 3 mm above the surface, beam inclined by 10° piercing.

2.2. Comparing the raw OCT measurement with the longitudinal section of the seam

The comparison of the acquired raw OCT data and the longitudinal section of the welded seam is shown in Fig. 4. The black points show the OCT measurements. The blue line shows the real depth of the produced seam which was determined from a longitudinal section of the welded seam. It can be seen that the surface before and after the welding process is measured precisely by OCT, but the depths measured during the welding process are scattered over a very broad range and do not directly and unambiguously reveal the correct welding depth.

Most of the measured points lie above and a small fraction below the actual welding depth, which is given by the bottom of the welded seam. Since it is unlikely that the capillary was deeper than this welding depth, the measurement points lying below the actual welding depth (blue line in Fig. 4) have either to be attributed to noise of the measurement system

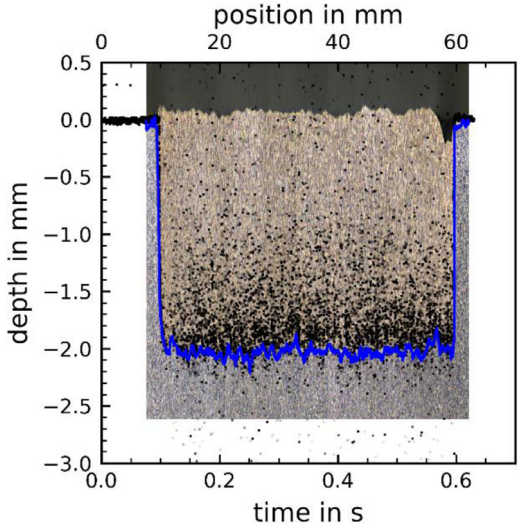

Fig. 4. Comparison of the longitudinal section of a welded seam (photographic image) with the raw data points of the OCT depth measurement (black dots) of example A. The blue line marks the actual welding depth, which is defined by the bottom of the seam observed in the longitudinal section. See parameters in Fig. 3.

or to a real elongation of the optical path length, either due to optical or geometrical effects (such as a bending of the vapor capillary with several reflections of the OCT probe beam). It should however also be noted that a minor amount of deviation can also result from the fact that the longitudinal section might not have been taken exactly from the middle of the weld seam.

3. Analysis of the OCT measurement signal

There are several approaches to process the measured data. A statistical approach using a percentile filter to determine the welding depth and the depth variance [28] was used here, whose viability was confirmed in [29,30]. An alternative method using a fit function on the histogram of the measured data is shown in [31].

The drawback of using a one-step filter method, is the need to adjust the filter parameters to every set of process parameters, mostly due to the different signal densities and noise characteristics of the measurements. It is therefore advantageous to first remove the noise and then apply the percentile filter to the cleaned measurement data.

3.1. Signal ranges of the measurements

When plotting the measured depth over time as shown in Fig. 5, the data points can be segmented in three main depth regions. The points within the region S are likely to origin from measurements of the surface, the region C encloses the range where the depth of the capillary is measured and, since the capillary cannot be deeper than the welding depth, the data points included in the range N must be considered to be noise.

Any filtering algorithm used to extract the welding depth should only consider measurements within the domains S and C. The measurement signal therefore first needs to cleaned from the measurements belonging to the noise domain N.

3.2. Segmentation of the signal regions

Two different approaches are presented in the following to segment the raw measurement data into two sets, one set containing the noise N and the other one containing the measurement of the surface and the length of the capillary.

3.2.1. Segmentation based on histogram

The histogram displaying how often (ordinate) the measured depth (abscissa) lies within a given depth (usually referred to as bin) interval

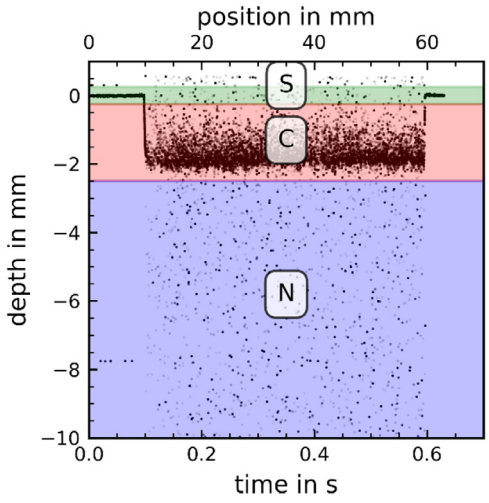

Fig. 5. Subdivision of the measurement results into three domains: S includes measurements of the surface, C the plausible depth of the capillary, and N is noise. (Example A) See parameters in Fig. 3.

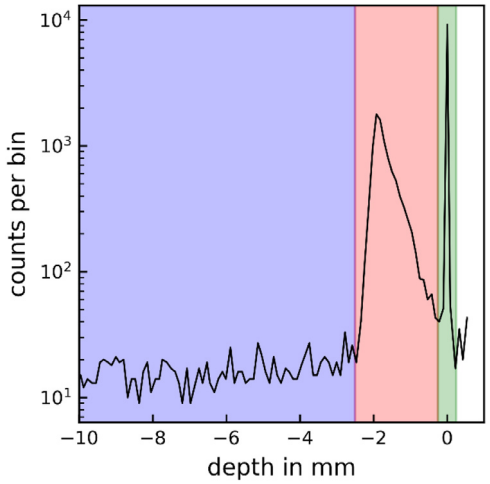

Fig. 6. Subdivision of the raw data based on the histogram of the number of measurements yielding a given depth, applied to the complete measurement data of example A. One bin equals 1/100 of the shown depth range. See processing parameters in Fig. 3.

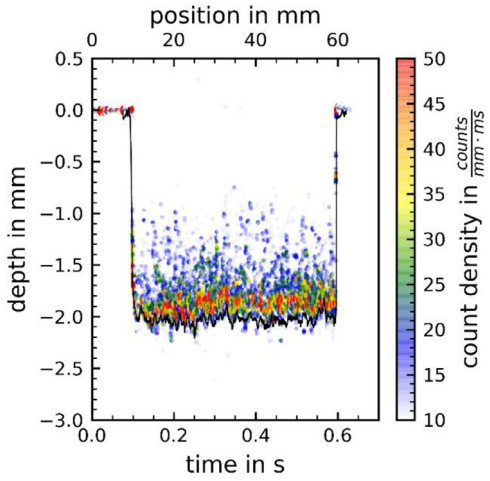

Fig. 7. Count density (color-coded) along the measurement of the welding depth over time (example A). For reference the actual seam depth is drawn in black. See processing parameters in Fig. 3.

is shown in Fig. 6, still for the so far discussed example A. The bin width was chosen to be one hundredth of the complete depth range. The counts per bin measured at depths deeper than −2.25 mm are much lower than at depths further above. The region with this low count therefore can be interpreted to be the domain N and the two distinct count peaks measured at shallower depths can be attributed to the domain C of the capillary and the domain S of the surface.

As seen from the histogram, the noise can be well separated from the relevant ranges C and S by means of a threshold for the number of counts per bin. This is also illustrated by Fig. 7, where the measurements are now additionally resolved in the time domain by showing the (color coded) count density, which reveals how frequently (per unit time) the measured depth lies within a given depth bin.

In this example a threshold of the count density of roughly $\frac{10}{mm \cdot ms}$ would be effective to discriminate the noise.

3.2.2. *Segmentation using the Poisson-distribution*

An alternative method to separate the noise from the measurement data is based on the Poisson-distribution which is common for the shot noise in optical sensors [32,33].

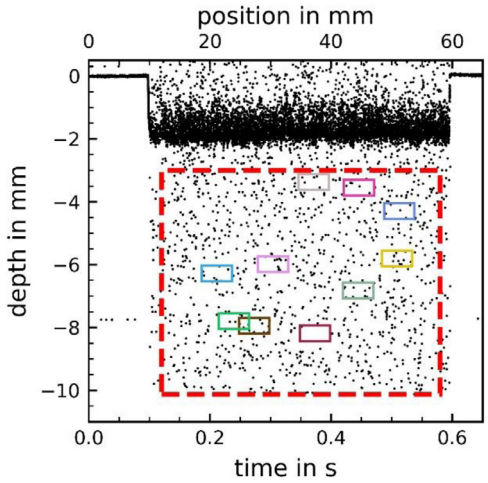

Fig. 8. The red dashed line indicates the area with only noise. The colored rectangles represent ten of 3000 areas where the counts were analyzed. (Example A), see processing parameters in Fig. 3.

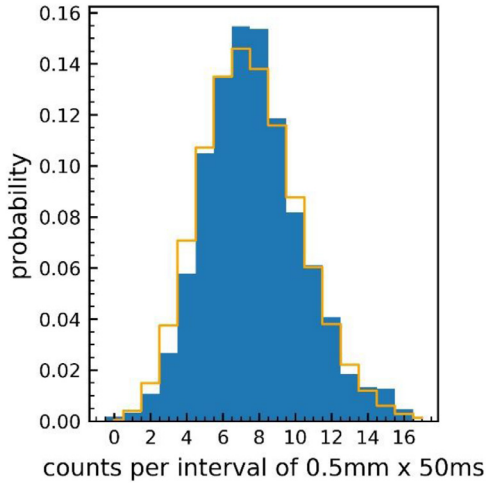

Fig. 9. Probability of the occurrence of a given number of counts per interval of 0.5 mm × 50 ms. Blue: measured by evaluating the number of counts in 3000 rectangles of 0.5 mm × 50 ms as indicated in Fig. 8. Orange: calculated using the Poisson distribution (1) with $\mu(0.5\ mm,\ 0.05\ s) = 7.56$. (Example A), see processing parameters in Fig. 3.

With the Poisson distribution, the probability to measure k counts in a given interval of depth $\Delta\delta$ and time Δt is given by

$$Poi(k, \mu) = e^{-\mu(\Delta\delta, \Delta t)} \cdot \frac{\mu(\Delta\delta, \Delta t)^k}{k!}, \tag{1}$$

where μ is the average count per interval [34].

In Fig. 8 the area with only noise is marked with a dashed red frame and ranges from −3 mm to −10 mm and from 0.12 s to 0.58 s. In total 991 data points were recorded within this (red dashed) rectangle. The average noise count density therefore is $\mu_N = 302.51 \frac{\text{counts}}{mm \cdot s}$.

For smaller areas as given by rectangles measuring $\Delta\delta$ in depth times Δt in time, the expected average number of counts is given by

$$\mu(\Delta\delta,\ \Delta t) = \mu_N \cdot \Delta\delta \cdot \Delta t. \tag{2}$$

For rectangles of 0.5 mm × 50 ms, such as indicated by the colored rectangles in Fig. 8, the average number of counts yields $\mu(0.5\ mm,\ 0.05\ s) = 7.56$. Fig. 9 shows a comparison of the probability to record a certain number of counts in such a small interval as calculated by Eq. (1) with $\mu(0.5\ mm,\ 0.05\ s) = 7.56$ (orange line), to the one determined by analyzing 3000 rectangles of 0.5 mm × 50 ms that were randomly placed within the red dashed rectangle shown in Fig. 8 (blue

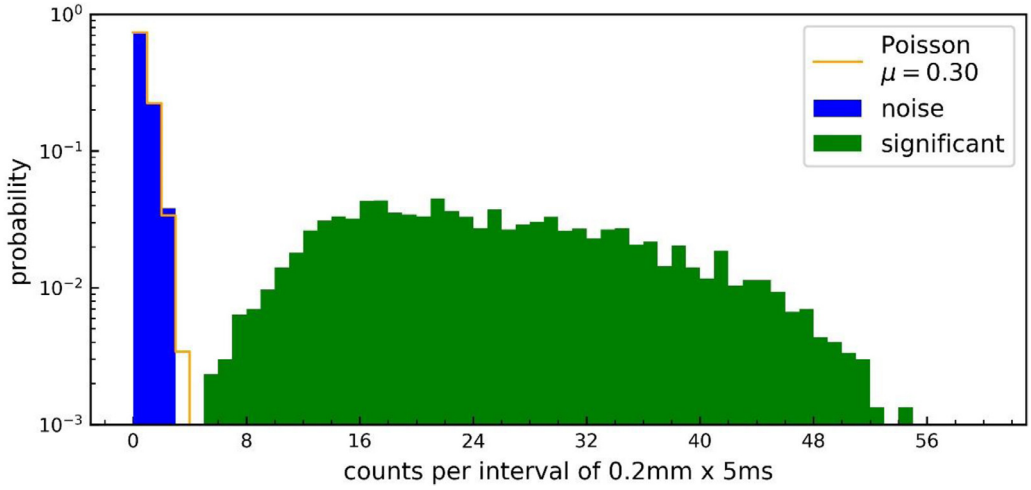

Fig. 10. Discrimination of noise (domain N, blue) and significant measurements of the capillary depth (domain C, green) by comparison of the measured counts probabilities to the Poisson distribution. The expected number of counts in the noise domain was $\mu(0.2\ mm,\ 0.005\ s) = 0.3$. (Example A).

columns). In the latter case the probabilities were determined by counting how many times a given number of measurements were contained in the individual rectangles divided by 3000. The agreement between the calculated and the measured distribution shows that the count of the measurements in the region N can well be expressed by the Poisson distribution.

Indeed, extending the evaluation to a larger area that spans a duration of 5 ms and a depth range from −2.1 mm to −1.5 mm—hence including part of the region C defined above—and determining the probability of counts occurring in small intervals of 0.2 mm × 5 ms, where $\mu(0.2\ mm,\ 5ms) = 0.3$, leads to the results shown in Fig. 10. This illustrates that a comparison of the measured probability to obtain a given number of counts in a given interval (of depth and time) to the one expected according to the Poisson distribution with μ as determined in the region N can be used to distinguish between noise and the significant measurement of the capillary depth. When the measured counts probability in a given interval (blue) corresponds to the one expected from the Poisson distribution (orange), the corresponding data points are assumed to be noise, in the other cases (green) it is considered to be the significant measurements of the capillary depth.

With known μ one can therefore define the noise probability per interval $\Delta\delta \cdot \Delta t$ by

$$N_P(k, \mu) = \frac{Poi(k, \mu(\Delta\delta,\ \Delta t))}{\max\limits_k \left(Poi(k, \mu(\Delta\delta,\ \Delta t))\right)}. \tag{3}$$

Thus the noise probability ranges from zero, when the number of counts k significantly deviates from what is expected for the noise, to one, when the regarded interval includes only noise and k therefore is close to μ. In the experiment, k is determined by counting the number of measurements within many regularly placed intervals with the extent $\Delta\delta \times \Delta t$.

Fig. 11 shows the noise probability $N_P(k,\ \mu(\Delta\delta, \Delta t))$ of the data from example A for a time interval stretching the whole welding time (0.2–0.6 s) as a function of the measured depth. The width of one depth bin here is 0.107 mm, hence $\mu(0.107\ mm,\ 0.4\ s) = 12.94$, which was determined in the range of −10 to −3 mm and 0.12 s to 0.58 s.

As expected, the probability of the measured depth to be just noise is the highest (almost 1) in the range N where the measured counts k per interval of 0.107 mm × 0.4 s is close to μ. In contrast, the noise probability of the depth measurements is low in the domains of the capillary (C) and the surface (S) of the workpiece where the counts k per interval are significantly higher than in the noise domain ($k \gg \mu$).

Resolving the noise probability (color coded) of the measured depth in the time domain with time intervals of 5 ms leads to the plot shown

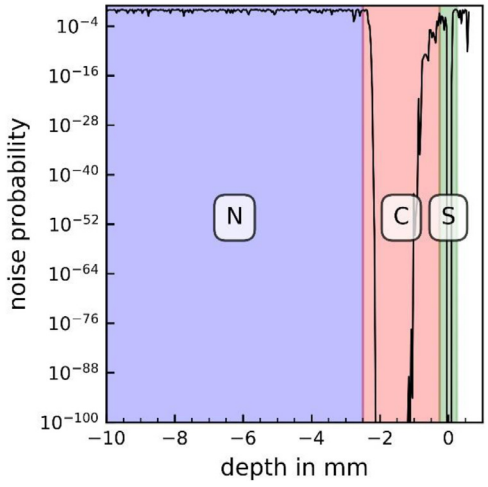

Fig. 11. Noise probability of the depth measurements of example A. Number of depth bins is 100 (width of the bins is 0.107 mm) and $\mu(0.107\ mm,\ 0.4\ s) = 12.94$.

in Fig. 12. As a reference, the actual welding depth is again drawn as a thin black line. It can be seen that the measurements yielding a depth of closely above the actual welding depth during the welding process and a depth of about zero (surface) before and after the process have a very low noise probability of less than 10^{-20} and can therefore be considered to be valid results.

The noise probability makes an excellent criterion to subdivide the raw measurement data into noise (domain N) and the significant depth signal. Choosing a suitable noise threshold value $N_{P,\ th}$ therefore allows to distinguish the measured noise with $N_P(k,\ \mu) \geq N_{P,\ th}$ from the significant measurements with $N_P(k,\ \mu) < N_{P,\ th}$. A noise threshold value of 10^{-5} was found to work for all considered measurements – originating from experiments using different materials (steel, aluminum, copper) and different welding parameters.

The same threshold value was used for the measurements in many different experiments to separate between the depth ranges N and C (during the welding process) or S (before and after the welding process). Two examples are shown Fig. 13: The black points represent the raw measurement data. The measurement points with a noise probability of less than 10^{-5} are marked in red and represent the significant information. Again as a reference, the blue line indicates the actual welding depth, which was extracted from longitudinal sections of the weld seam. The plot on the left still shows example A. The plot on the right

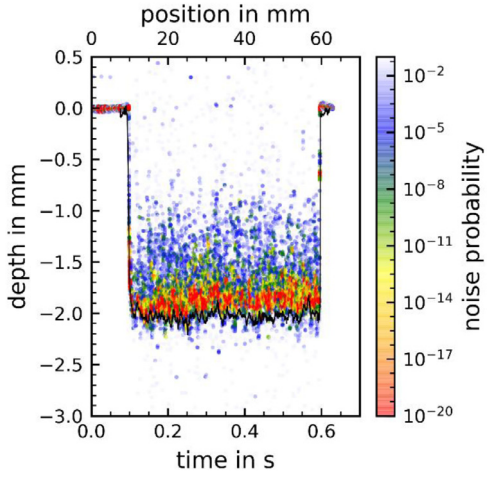

Fig. 12. Noise probability (color coded) along the time-resolved depth measurements of example A. The actual seam depth is drawn in black as a reference. The expected noise counts per interval was $\mu(0.107\ mm,\ 0.005\ s) = 0.08$.

resulted by applying the same filtering method to a different welding process, where aluminum was used as the sample material, applying a laser power of 4 kW and a feed rate of 4 m/min. The method reliably discriminates the significant depths signal against the noise in both cases.

The segmentation using the noise probability works for different welding situations and was therefore used to extract the data for the further treatment as described below. The used parameters where $N_{P,th} = 10^{-5}$and the expected count was $\mu(0.107\text{mm},\ 0.005\ \text{s}) = 0.08$ on the left side and $\mu(0.107\text{mm},\ 0.005\ \text{s}) = 0.08$ on the right side.

3.3. Data refining: percentile filter on domain C

After the separation of the measurement noise from the significant data, a sophisticated filtering method has to be applied to extract the actual welding depth.

Compared to other filtering methods such as averaging, it was found that the application of the percentile filter leads to results that exhibit the best agreement with the actual seam depth. Only this approach is therefore discussed in the following.

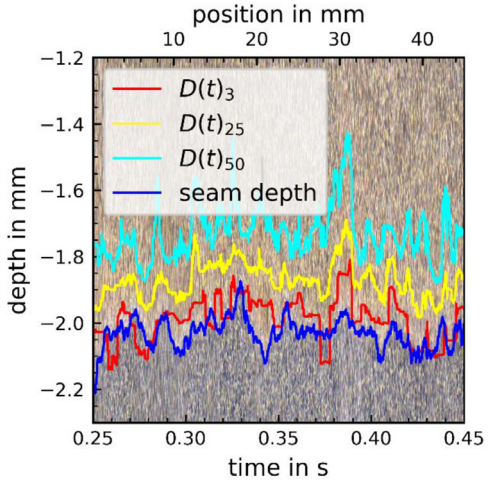

Fig. 14. Depths extracted from the measurements previously identified to be significant data by applying the percentile filters $p = 3$, $p = 25$ (quartile) and $p = 50$ (median) compared to the actual seam depth obtained from a longitudinal section of the welded seam (example A). The window-length used for the percentile filtering was $\tau = 5$ ms.

The filter is used in a running manner with a centered flat window. At each discrete measurement time t_i all the measurements recorded at the times

$$\mathbf{T}_i = \left[\ t_i - \frac{\tau}{2}, t_i - \frac{\tau}{2} + \Delta t, \ldots,\ t_i + \frac{\tau}{2}\right] \tag{4}$$

are taken into account, where τ is the filter window size, and $\Delta t = 1/f$ the period between two depth measurements (f being the sampling rate of the OCT detector). The filtered depth is obtained by applying a percentile filter [35] on the depths $D(t_i)$ measured at the discrete times of the set $\mathbf{T}_i$,

$$D\left(t_i\right)_p = F\left[D(t),\ t \in \mathbf{T}_i\right] \tag{5}$$

which means that p percent of all measured depths are smaller than the value $D(t_i)_p$.

Applying the percentiles $p = 50$ (median), $p = 25$ (quartile) and $p = 3$ only to the measured depth previously identified as belonging to the significant data of example A, yields the filtered depths traces shown in Fig. 14.

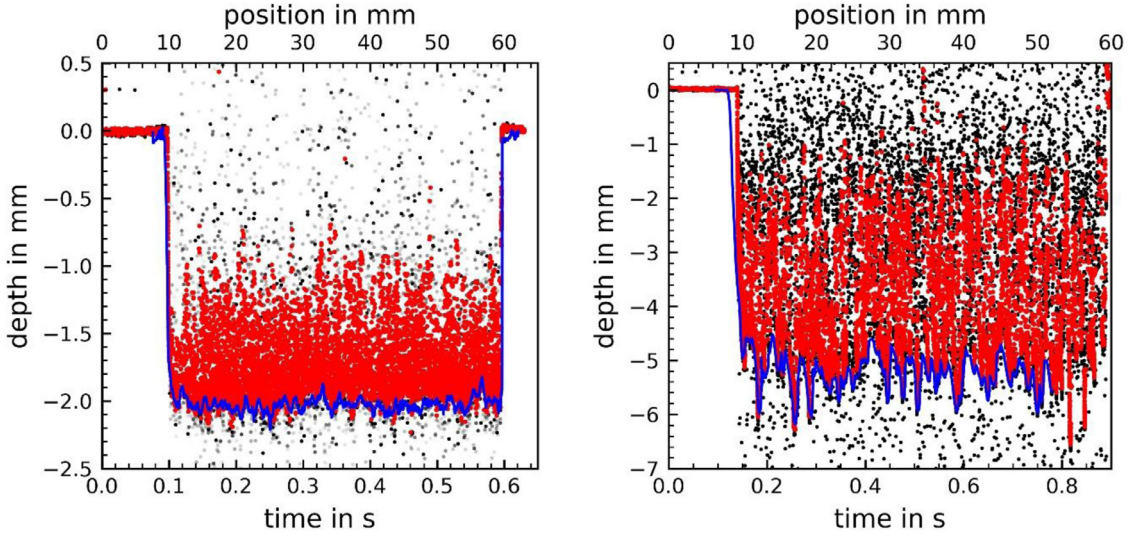

Fig. 13. Discrimination of the measurement points with significant information on the welding depth (red) against the measurement noise (black). As a reference the blue lines indicate the actual welding depth as obtained from longitudinal sections along the welded seam. Left: example A. Right: same filtering algorithm applied to a different welding process with the same laser setup but welding aluminum with a power of 4 kW and a feed rate of 4 m/min. The expected count was $\mu(0.107\ mm,\ 0.005\ s) = 0.08$ on the left and $\mu(0.107\ mm,\ 0.005\ s) = 0.096$ on the right.

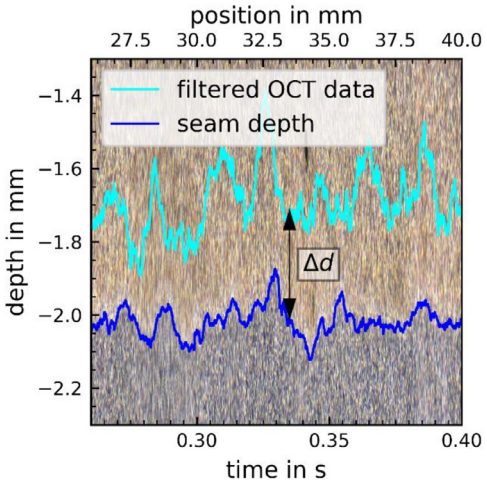

Fig. 15. The difference between the depth extracted from the OCT data to the actual seam depth obtained from longitudinal section of the welds was used to assess the data evaluation method.

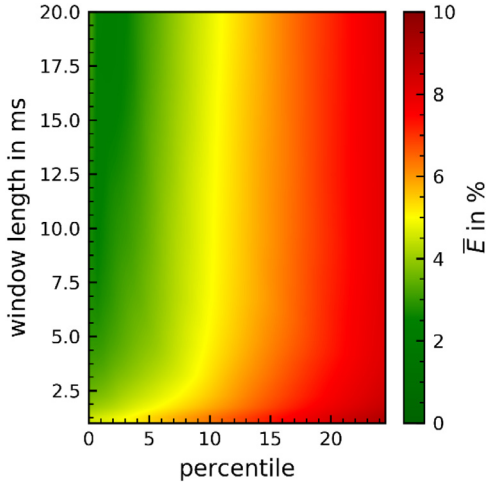

Fig. 16. Dependence of the averaged error E (color coded) on the percentile p and the window length τ applied to extract the welding depth form the OCT signal of example A. Poisson pre-filter parameters: $\mu(0.107\ mm,\ 0.005\ s) = 0.08$, threshold $N_{P,th} = 10^{-5}$.

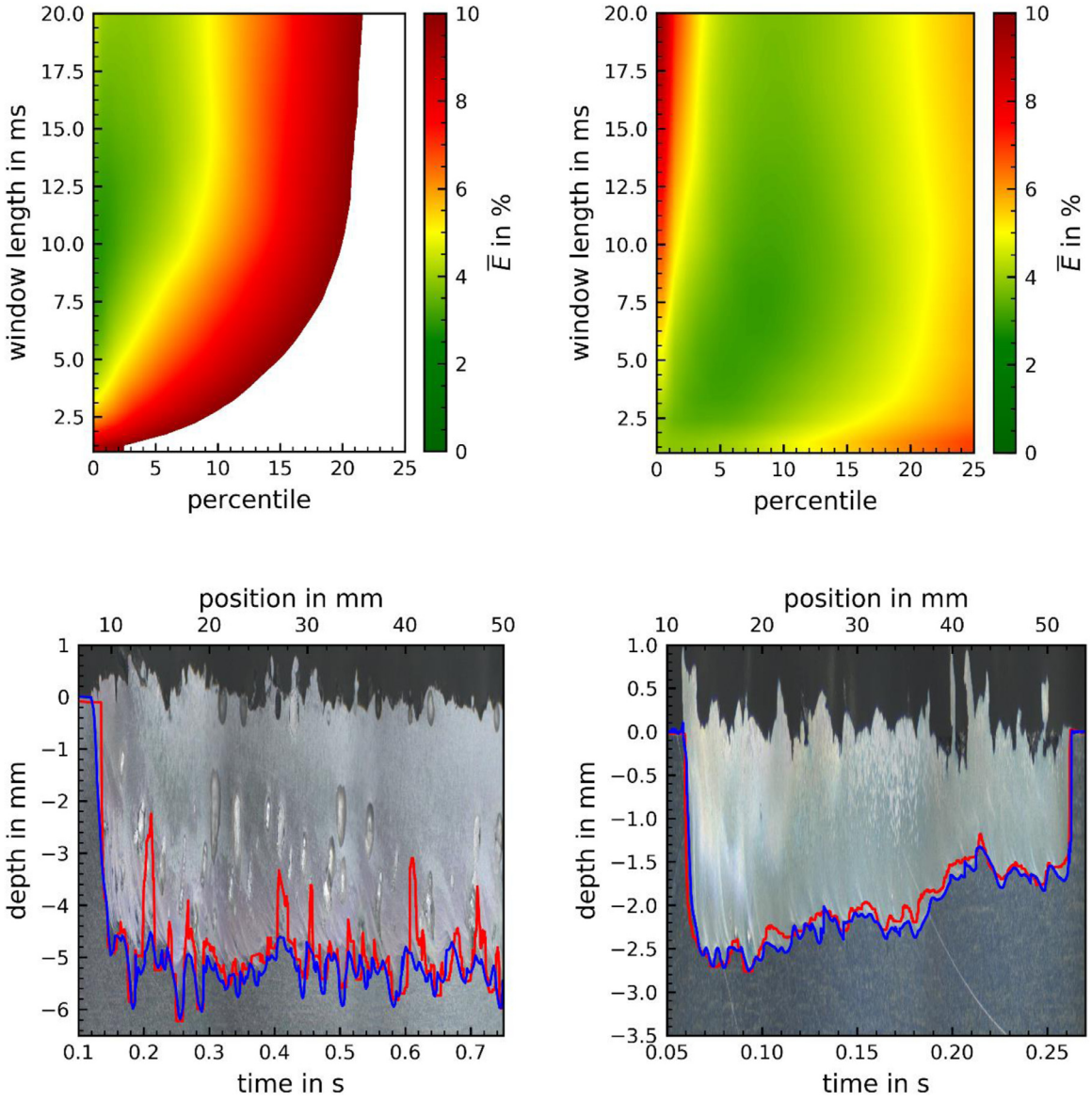

Fig. 17. Top: Average Error E. Bottom: depth extracted from the OCT signal (red) using $p = 3$ with $\tau = 5$ ms and actual seam depth (blue). Welding of aluminum with the laser parameters: $P_L = 4$ kW, $D_f = 300$ µm (150 µm fiber, NA = 0.1), v = 4 m/min (left) or v = 12 m/min (right).

In this example the depths extracted with $p = 3$ agree best with the acutal welding depth. It was observed that a percentile filter with percentiles well below 25 should be used to obtain viable results.

3.4. Suitable setting of percentile and window length

In order to assess the performance of the proposed evaluation method and to determine the best suited settings for the percentile filtering, the difference Δd between the depth values extracted from the OCT signal to the actual seam depth as extracted from longitudinal sections through the welds was considered, as indicated in Fig. 15.

The average error

$$E = \frac{\sum_{i=0}^{n} |\Delta d_i|}{n \cdot \bar{D}}, \tag{6}$$

where Δd_i are the differences between the measured depth and the actual seam depth at the discrete measurement times t_i, n is the number of considered measurement points, and $\bar{D}$ is the average seam depth, only including weld seam depths $\neq 0$, was used to quantify the accuracy of the extracted depths. This definition reflects the mean offset of every measured depth and might be caused by a constant systematic offset, spikes in both directions, or oscillations around the weld seam depth.

The percentile filter has two parameters, the window length τ and the percentile p. Both can be adapted to minimize the average error E.

Fig. 16 shows the average depth error E in percent (color coded) as a function of the used percentile p and window length τ. Obviously a low percentile yields smaller errors, whereas the window length has a minor influence provided that it exceeds about 3 ms.

An error of less than 5% of the mean depth of the seam can be achieved with percentiles of below 10 and a window length between 3 and 20 ms. It can be recommended to use a percentile between $p = 2$ and $p = 5$, resulting in errors of less than 5%. It is advisable not to use $p = 0$ (minimum) since any noise that passes the filter will then be considered as a valid measurement of the welding depth. As shown by the experimental validation below, these values can be taken as a general reference.

4. Experimental validation

The evaluation method presented above to extract the welding depth from the raw OCT data was tested on a series of welding experiments that where performed with different conditions and parameters. Fig. 17 shows the measured depths (bottom) as well as the

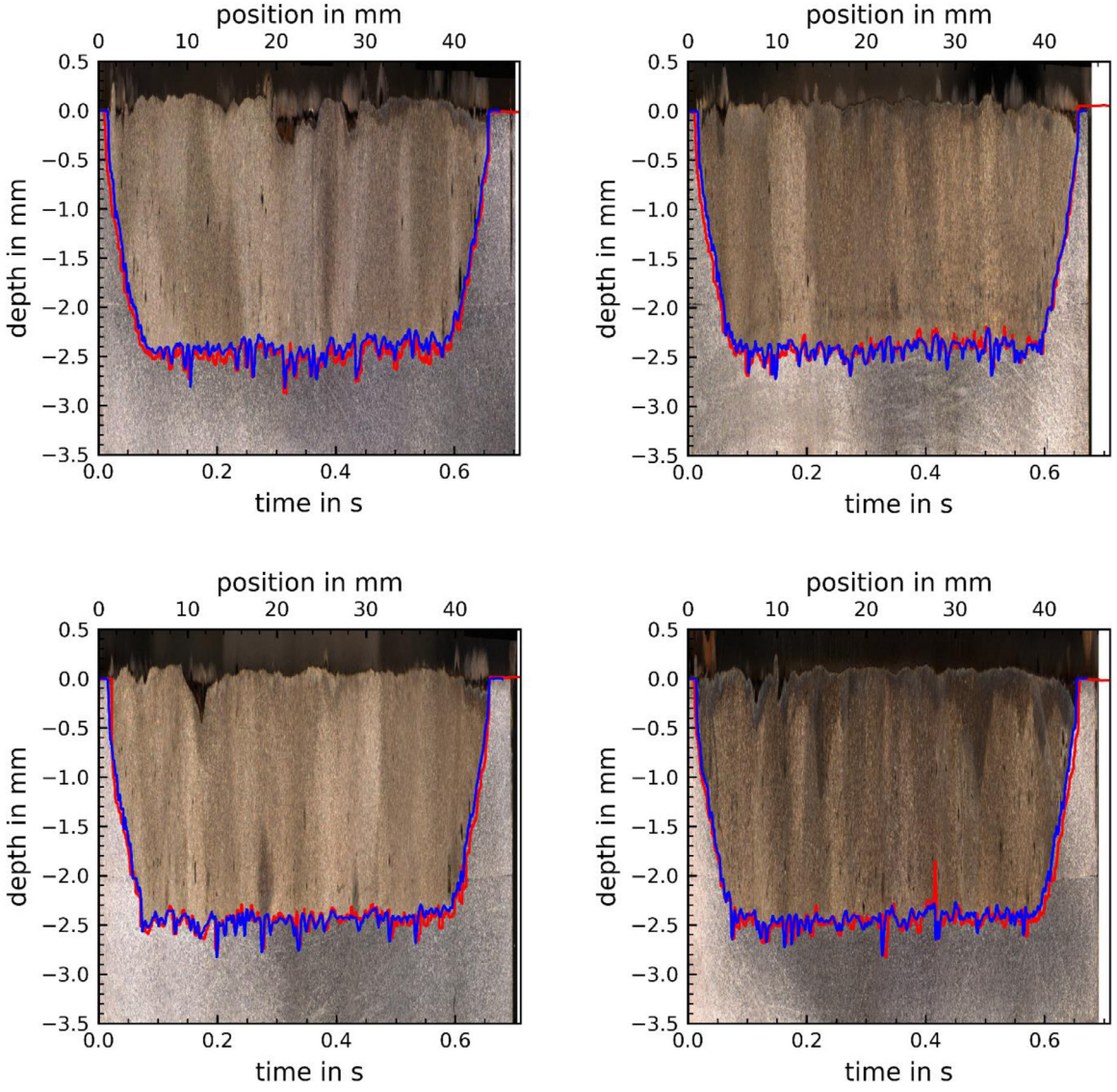

Fig. 18. Comparison of welding depth extracted from the OCT measurement ($p = 3$, $\tau = 5$ *ms*) in red and the actual seam depth according to the longitudinal sections of the welds (blue). Four experiments performed with the same process parameters (Mild steel, $P_L = 1.5$ kW, v = 4 m/min, $D_f = 200$ µm, $d_{fiber} = 150$ µm, $NA_{fiber} = 0.1$, nitrogen as assist gas).

influence of the filtering parameters on the error resulting average error (top). In both cases (left and right) the measurements result from welding aluminum with 4 kW of laser power (P_L) with the laser beam focused onto the surface of the workpiece using setup A. The feed rate (v) was changed from 4 m/min (left) to 12 m/min (right). In both cases the use of a percentile of 2% to 5% with a window length of 5 ms results in an error of less than 5% of the average seam depth. Apart from the individual spikes that are common for the typically dynamic welding processes in aluminum, the longitudinal sections at the bottom of Fig. 17 show a very good agreement between the welding depth extracted from the OCT data with the actual weld seam. The spikes could be dealt with separately to improve the accuracy even more, for example by additionally filtering out “upward” spikes of a certain height when processing the OCT signal.

To further prove the repeatability of the proposed filtering technique, multiple welds with constant parameters were performed to join two sheets of mild steel with a thickness of 2 mm each in overlap configuration. The Laser power was set to 1.5 kW and the feed rate to 4 m/min. Nitrogen was applied as the shielding gas.

Fig. 18 shows the depth extracted from the OCT ($p = 3$, $\tau = 5\ ms$) in red and the actual seam depth in blue. The difference between the curves is very small, the average error was less than 100 µm for all examples.

The accuracy of the depth extracted from the OCT measurement is remarkably high. Using the same unchanged filtering parameters for all shown examples, the average error was less than 5%. The proposed pre-filtering to clean the significant measurement date from the noise eliminates the need to adapt the filter parameters to every welding condition.

5. Conclusion

In conclusion we have proposed a method to reliably extract the welding depth from OCT measurements recorded during laser welding. It was found that the noise can be separated from the significant measurements by analyzing the frequency of measurements in a given depth interval. This is done by first determining the count rates that are typical for the noise signal. Using this value as the event rate in the Poisson distribution allowed to define a probability to reliably distinguish between the significant measurements and noise.

A running percentile filter was then used to extract the welding depth from the measurements that were cleaned from the noise contribution. It was found, that using a window length in the range of 5–20 ms and a percentile of 2%–5%, yields a measured depth that agrees well with the weld seam depth and that these settings are useful for different welding conditions.

Hence, the optical coherence tomography can be a viable tool to measure the seam depth during deep-penetration laser welding. The high achievable accuracy makes the OCT technique a convenient tool for quality assurance in industrial applications and may potentially be further developed to implement a closed-loop depth control for laser beam welding.

References

[1] Müller MG. Prozessüberwachung beim laserstrahlschweißen durch auswertung der reflektierten leistung. Herbert: Utz Verlag; 2002.

[2] . Integration optischer messmethoden zur prozesskontrolle beim laserstrahlschweissen (iness): abschlussbericht zum verbundprojekt. Integration optischer messmethoden zur prozesskontrolle beim laserstrahlschweissen (iness): abschlussbericht zum verbundprojekt. Müller-Borhanian J, editor. München: Utz Verlag; 2005.

[3] Weberpals J.P., Stritt P., Weber R., Thiel C., Abt F., Michalowski A. Verfahren zum bestimmen einer bearbeitungstiefe einer lasergestützten materialbearbeitung(DE102014007074); 2014; Available from: https://worldwide.espacenet.com/publicationDetails/biblio?CC=DE&NR=102014007074B3&KC=B3&FT=D#.

[4] Birnesser AJ. Prozessregelung beim laserstrahlschweißen. München: Utz Verlag; 2011.

[5] Lahdo R, Seffer O, Kaierle S, Overmeyer L. In-process control of penetration depth for high-power laser welding of thick dissimilar joints of steel and aluminum. In: Laser Institute of America, editor. Proceedings of ICALEO 2018; 2018.

[6] Abt F, Blug A, Nicolosi L. Analoge bildverarbeitung mit cellularen neuralen netzen (CNN) zur regelung laserbasierter schweißprozesse—ACES.: abschlussbericht zum projekt aces gefördert von der badenwürttembergstiftung; 2011. Stuttgart, Freiburg, Dresden.

[7] Abt F. Bildbasierte charakterisierung und regelung von laserschweißprozessen, München: Herbert Utz Verlag; 2017. Wissenschaft.

[8] Tomlins PH, Wang RK. Theory, developments and applications of optical coherence tomography. J Phys D 2005;38(15):2519.

[9] Fercher AF, Drexler W, Hitzenberger CK, Lasser T. Optical coherence tomography-principles and applications. Rep Prog Phys 2003;66(2):239.

[10] Precitec. Precitec IDM. [July 10, 2018]; Available from: http://www.precitec.de/produkte/fuegetechnologie/prozessueberwachung/precitec-idm/.

[11] Dutton HJR. Understanding optical communications. Upper saddle river. N.J: Prentice Hall PTR; 1998.

[12] Miyagi M, Kawahito Y, Kawakami H, Shoubu T. Dynamics of solid-liquid interface and porosity formation determined through x-ray phase-contrast in laser welding of pure Al. J Mater Process Technol 2017;250:9–15.

[13] Callies G, Schittenhelm H, Berger P, Huegel H, Pinho GP. Condensation phenomena and refraction index distributions in excimer laser-induced plasma/vapor plumes. In: International society for optics and photonics; 1997. p. 398–402.

[14] Oiwa S, Kawahito Y, Mizutani M, Katayama S. Effect of atmosphere above specimen on welding results during remote welding. J Laser Appl 2011;23(2):22007.

[15] Zou J, Yang W, Wu S, He Y, Xiao R. Effect of plume on weld penetration during high-power fiber laser welding. J Laser Appl 2016;28(2):22003.

[16] Matsunawa A, Kim J-D, Takemoto T, Katayama S. Spectroscopic studies on laser induced plume of aluminum alloys. In: Mazumder J, editor. Proceedings of the Laser Materials Processing Conference: November 13–16, 1995. LIA Laser Inst. of America; 1995. p. 719–28.

[17] Kawahito Y, Kinoshita K, Matsumoto N, Katayama S. Visualization of refraction and attenuation of near-infrared laser beam due to laser-induced plume. J Laser Appl 2009;21(2):96–101.

[18] Kawahito Y, Matsumoto N, Mizutani M, Katayama S. Characterisation of plasma induced during high power fibre laser welding of stainless steel. Sci Technol Weld Join 2008;13(8):744–8.

[19] Zhang M, Chen G, Zhou Y, Li S. Direct observation of keyhole characteristics in deep penetration laser welding with a 10 kW fiber laser. Optics Express 2013;21(17):19997–20004.

[20] Bautze T. Keyhole depth is just a distance. LTJ 2014;11(4):39–43.

[21] Webster PJL, Wright LG, Ji Y, Galbraith CM, Kinross AW, van Vlack C, et al. Automatic laser welding and milling with in situ inline coherent imaging. Opt Lett 2014;39(21):6217–20.

[22] Blecher JJ, Galbraith CM, van Vlack C, Palmer TA, Fraser JM, Webster PJL, et al. Real time monitoring of laser beam welding keyhole depth by laser interferometry. Sci Technol Weld Join 2014;19(7):560–4 Volume 19, Issue 7.

[23] Laser Depth Dynamics. Laser Depth Dynamics Website. [July 10, 2018]; Available from: http://www.laserdepth.com/applications/.

[24] Kogel-Hollacher M, Schoenleber M, Bautze T, Strebel M, Moser R. Measurement and closed-loop control of the penetration depth in laser materials processing. 9th international conference on photonic technologies LANE; 2016.

[25] Webster Paul JL, Galbraith CM, Vlack Cole Van, Buckley DR, Fraser JM. Three-dimensional, multi-factor monitoring and control of laser keyhole welding by inline coherent imaging; 2015. München.

[26] Webster PJL, Muller MS, Fraser JM. High speed in situ depth profiling of ultrafast micromachining. Opt Express 2007;15(23):14967.

[27] Webster PJL, Leung BYC, Yu JXZ, Anderson MD, Hoult TP, Fraser JM. Coaxial real-time metrology and gas assisted laser micromachining: process development, stochastic behavior, and feedback control. MOEMS-MEMS. Maher MA, Chiao J-C, Resnick PJ, editors. SPIE; 2010.

[28] Boley M., Berger P., Webster, P.J.L., Weber R., van Vlack, C.V. Fraser J. et al. Investigating the weld depth behaviour using different observation techniques: x-ray, inline coherent imaging and highspeed observation of ice. ICALEO 2013:22–7.

[29] Authier N, Baptiste A, Bruyere V, Namy P, Touvrey C. Implementation Of An Interferometric Sensor For Measuring The Depth Of A Capillary Laser WeldinG: paper 904. In: Laser Institute of America, editor. Proceedings of ICALEO 2016; 2016.

[30] Bono Pde, Allen C, D'Angelo G, Cisi A. Investigation of optical sensor approaches for real-time monitoring during fibre laser welding: paper Number 1504. In: Laser Institute of America, editor. Proceedings of ICALEO 2016; 2016. p. 22417.

[31] Dorsch F, Harrer T, Haug P, Plasswich S. Process control using capillary depth measurement. In: Laser Institute of America (Hg.) 2016— Proceedings of ICALEO; 2016.

[32] . Machine vision handbook. Machine vision handbook. Batchelor BG, editor. London: Springer; 2012.

[33] Schottky W. Über spontane Stromschwankungen in verschiedenen Elektrizitätsleitern. Ann. Phys. 1918;362(23):541–67.

[34] Yates RD, Goodman DJ. Probability and stochastic processes: a friendly introduction for electrical and computer engineers. 2nd ed. Hoboken, NJ: Wiley; 2005.

[35] The SciPy community. numpy.percentile. [February 25, 2019]; Available from: https://docs.scipy.org/doc/numpy/reference/generated/numpy.percentile.html.